Electromagnetic scattering by a partially graphene-coated dielectric cylinder: Efficient computation and multiple plasmonic resonances

Youssef Jeyar,[1] Mauro Antezza,[1,2] and Brahim Guizal[1,*]

[1]*Laboratoire Charles Coulomb (L2C), UMR 5221 CNRS-Université de Montpellier, F-34095 Montpellier, France*

[2]*Institut Universitaire de France, 1 rue Descartes, Paris Cedex 05 F-75231, France*

(Received 20 June 2022; revised 10 January 2023; accepted 7 February 2023; published 23 February 2023)

We present a numerical approach for the solution of electromagnetic scattering from a dielectric cylinder partially covered with graphene. It is based on a classical Fourier-Bessel expansion of the fields inside and outside the cylinder to which we apply *ad hoc* boundary conditions in the presence of graphene. Due to the singular nature of the electric field at the edges of the graphene sheet, we introduce auxiliary boundary conditions. The result is a particularly simple and efficient method allowing the study of diffraction from such structures. We also highlight the presence of multiple plasmonic resonances that we ascribe to the surface modes of the coated cylinder.

DOI: 10.1103/PhysRevE.107.025306

I. INTRODUCTION

Scattering of electromagnetic waves from a dielectric or a metallic circular cylinder is rather a simple and classical problem [1]. In this situation, the incoming and outgoing fields can be represented in terms of cylindrical waves expressed through Fourier-Bessel expansions, and all the channels are independent because of the circular symmetry and homogeneity of the cylinder. Usually, when the wavelength of the incoming wave is much larger than the diameter of the cylinder (this is the *subwavelength regime*), the wave is barely scattered. Interestingly, it has been shown that when cylindrical structures involve plasmonic materials (noble metals or graphene) they are able to exhibit quite unusual phenomena, such as superscattering [2,3] (i.e., they scatter light as if they were much larger than their actual size) and/or invisibility (i.e., they scatter light as if they were much smaller than their actual size). Furthermore, when the cylinder is partially covered with a perfect rectric conductor circular strip [4] or a circular strip of graphene [5,6], this breaks the symmetry and homogeneity at the level of the surface, and then all the channels can be mixed up leading to much richer physical behavior. In Ref. [5], an integral equation approach, based on the solution of the integral equation for the current induced on the graphene strip, has been used to explore the interplay between plasmonic-resonances and photonic-jet effects in terahertz (THz) wave scattering by a graphene-covered dielectric cylinder. The same approach has been used in Ref. [6] to study the performances of the THz antenna made of a circular dielectric rod with conformal strip of graphene.

Among the numerical methods used to solve electromagnetic problems, one can distinguish: (i) general methods, such as the finite difference time domain [7] or the finite elements method [8] capable of handling a vast variety of configurations but at the expense of time and memory consuming; and (ii) special methods specifically designed for certain configurations exploiting periodicity and/or symmetries, for example. These latter prove to be very efficient and much less time and memory consuming. It is this last kind of methods, we are going to rely on in solving the problem of scattering from a dielectric cylinder partially dressed with a graphene strip. Thus, we are going to use the periodicity of the conductivity function and introduce its Fourier expansion directly in the boundary conditions. After projection on the Fourier basis, this leads to an algebraic system linking the outgoing amplitudes of the fields to the incoming ones.This approach will be called the Fourier modal method (FMM) since it is the counterpart (or an extension) of the well known namesake method introduced for planar strips gratings [9,10]. In this very context (that of strip gratings), this method works extremely well in the case of transverse electric polarization, the electric field is parallel to the direction of invariance of the grating, but, unfortunately, may face serious convergence problems in the case of transverse magnetic (TM) polarization, the magnetic field is parallel to the direction of invariance of the grating. This is due to the fact that the tangential component of the electric field at the edges of the graphene sheet is null, hence, preventing from using the correct Fourier factorization rules [10,11] (cf. Sec. II B). In Ref. [10] Khavasi proposed a strategy to improve the situation through the introduction of approximate boundary conditions (ABCs) allowing the use of the correct Fourier factorization rules. This approach (that we will call FMM-ABC) shows a certain efficiency but does not completely fix the problem of convergence, especially for structures involving sharp resonances. Moreover, the technique introduces a new free parameter whose tweaking is very delicate [12]. It is also important to emphasize that the tangential electric field is singular in the vicinity of the graphene strips edges and is at the origin of the slow convergence for both the classical FMM and the FMM-ABC. Very recently, an alternative approach has been put forward by Hwang [12] in order to solve this issue. It is based on the use of a supplementary expression of the tangential electric field, right at the level of the interface, under the form of a special expansion in terms of local basis functions (LBF) able to reproduce the

*Corresponding author: brahim.guizal@umontpellier.fr

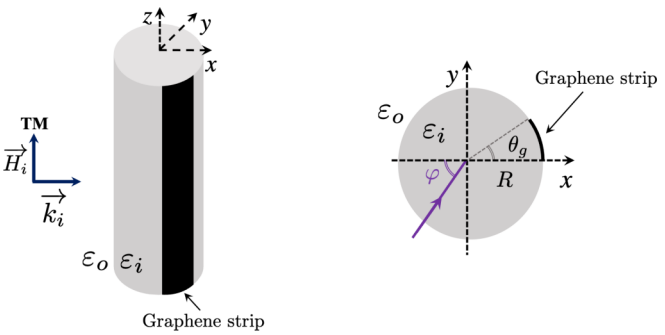

FIG. 1. Sketch of the diffraction problem under consideration: an electromagnetic plane wave hits the covered dielectric cylinder under classical diffraction, i.e., the incident wave vector is perpendicular to the direction of invariance oz.

aforementioned singularities (hereafter, this method will be called FMM-LBF). This proved to be extremely efficient not only from the standpoint of convergence of the efficiencies, but also in the representation of the field around the graphene strips.

In this paper, we introduce (in Sec. II) the FMM in the context of scattering by a dielectric cylinder partially covered with graphene as well as its FMM-ABC and FMM-LBF extensions. In Sec. III, we examine the convergence and stability of these three approaches and show the superiority of the FMM-LBF. Finally, we exploit the latter to highlight the presence of multiple resonances in the scattering efficiency spectrum for partially graphene-covered dielectric cylinders (on the contrary of what is observed for fully and homogeneously graphene-covered cylinders) and link them to the plasmonic surface modes over the structure.

II. THEORETICAL FRAMEWORK

The physical problem under study is depicted in Fig. 1 where a TM (magnetic field parallel to the direction of invariance oz), linearly polarized electromagnetic plane wave with vacuum wavelength λ illuminates a dielectric cylinder (radius R and relative dielectric permittivity ε_i) under classical incidence (the incident wave vector is perpendicular to oz) with an angle φ. The cylinder lies in a host medium (relative dielectric permittivity ε_o) and may be covered with graphene strips whose electromagnetic behavior is captured through their surface optical conductivity $\sigma(\omega)$. Both media are supposed nonmagnetic (relative magnetic permeabilities $\mu_{i/o} = 1$). In the following, we will use harmonic Maxwell's equations with the time convention $e^{-i\omega t}$.

Following Ref. [13], the graphene conductivity $\sigma(\omega)$ can be written as a sum of interband and intraband contributions, respectively, given by

$$\sigma_R(\omega) = \frac{i}{\omega + i\Gamma}\frac{2e^2 k_B T}{\pi\hbar^2}\ln\left(2\cosh\frac{\mu}{2k_B T}\right),$$
$$\sigma_I(\omega) = \frac{e^2}{4\hbar}\left[G\left(\frac{\hbar\omega}{2}\right) + i\frac{4\hbar\omega}{\pi}\int_0^{+\infty}\frac{G(\xi) - G\left(\frac{\hbar\omega}{2}\right)}{(\hbar\omega)^2 - 4\xi^2}d\xi\right], \quad (1)$$

$G(x) = \sinh(x/k_B T)/[\cosh(\mu/k_B T) + \cosh(x/k_B T)]$, T is the graphene strip temperature, $\Gamma = 2\pi/\tau$, τ being the relaxation time, and μ being the chemical potential.

In cylindrical coordinates, the z components of magnetic fields in the inner and outer media can be written in terms of the elementary Fourier-Bessel solutions [1],

$$H_{zo}(r,\theta) = \sum_n \{a_n J_n(k_o r) + b_n H_n^+(k_o r)\}e^{in\theta},$$
$$H_{zi}(r,\theta) = \sum_n c_n J_n(k_i r)e^{in\theta}, \quad (2)$$

where $k_{i/o} = k_0 n_{i/o}$ with $k_0 = 2\pi/\lambda$ and $n_{i/o} = \sqrt{\varepsilon_{i/o}}$, J_n and H_n^+ being the nth order Bessel and Hankel functions of the first kind, respectively ($n \in \mathbb{Z}$). Here $a_n = (ie^{-i\varphi})^n$ are the coefficients of the incident wave, whereas b_n and c_n are the scattering coefficients to be determined and from which all the physical quantities of interest can be readily computed. In the following, we will be mostly interested by the scattering efficiency, the expression of which is given by

$$Q_s = \frac{2}{k_o R}\sum_n |b_n|^2. \quad (3)$$

The determination of b_n and c_n is accomplished via the boundary conditions at $r = R$: $H_{zo}(R,\theta) - H_{zi}(R,\theta) = \sigma E_{\theta i}(R,\theta)$ and $E_{\theta i}(R,\theta) = E_{\theta o}(R,\theta)$ for all $\theta \in [0, 2\pi]$, where $E_{\theta i/o} = (-iZ_0/k_0\varepsilon_{i/o})\partial_r H_{zi/o}$ (Z_0 being the impedance of vacuum). Once projected on the Fourier basis $(e^{in\theta})_{n\in\mathbb{Z}}$,[1] these equations will furnish a set of algebraic equations linking the unknown coefficients to those representing the incident field. When the cylinder is fully and homogeneously covered with graphene, applying the aforementioned procedure leads to the following simple formulas of the scattering coefficients:

$$b_n = \frac{n_i J_{ni} J'_{no} - n_o J_{no} J'_{ni} + i\eta J'_{ni} J'_{no}}{n_o H_n^+ J'_{ni} - n_i J_{ni} H_n^{+'} - i\eta J'_{ni} H_n^{+'}} a_n,$$
$$c_n = \frac{n_i}{n_o}\frac{1}{J'_{ni}}\left\{J'_{no} a_n + H_n^{+'} b_n\right\}, \quad (4)$$

where $J_{n(i/o)} = J_n(k_{i/o}R)$, $J'_{n(i/o)} = J'_n(k_{i/o}R)$, $H_n^+ = H_n^+(k_o R)$, $H_n^{+'} = H_n^{+'}(k_o R)$, $\eta = Z_0\sigma(\omega)$, and where the primes denote the derivation with respect to variable r.

A. The classical FMM

If the cylinder is partially covered with graphene, one can use the classical FMM [4,9] where the conductivity function is expanded into Fourier series with respect to variable θ ($\sigma(\theta) = \sum_p \sigma_p e^{ip\theta}$) and inserted into the boundary conditions, which leads to the following expressions for the scattering coefficients:

$$b = B^{-1}a,$$
$$c = \frac{n_i}{n_o}J_i'^{-1}\{J'_o a + H^{+'} b\}, \quad (5)$$

[1]Throughout the paper, we use the classical inner product : $\langle f, g\rangle = \frac{1}{2\pi}\int_0^{2\pi} f(\theta)g^*(\theta)d\theta$, the asterisk indicating complex conjugation.

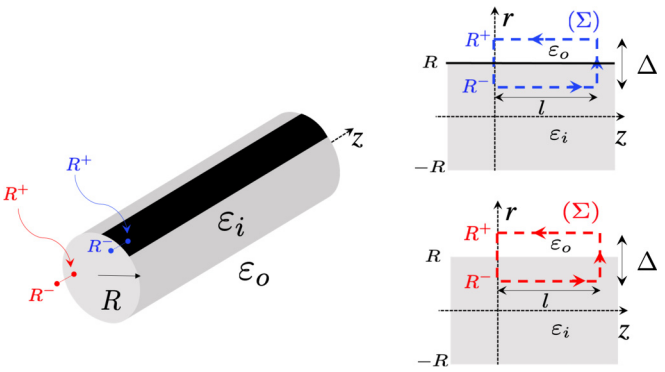

FIG. 2. Sketch of the contours used to derive the ABC. Top Right: A contour across graphene and bottom right: a contour on a bare part of the cylinder.

where matrices A and B are given by

$$A = n_i J_i J_o' - n_o J_o J_i' + iZ_0 J_i' \Sigma J_o',$$
$$B = n_o H^+ J_i' - n_i J_i H^{+'} - iZ_0 J_i' \Sigma H^{+'}, \tag{6}$$

where we introduced vectors $a, b, c = (a_n, b_n, c_n)_{n\in\mathbb{Z}}$ and diagonal matrices $J_{i/o} = \mathrm{diag}(J_{n(i/o)})$, $H^+ = \mathrm{diag}(H_n^+)$, $J'_{i/o} = \mathrm{diag}(J'_{n(i/o)})$, $H'^+ = \mathrm{diag}(H_n'^+)$. Σ is the Toeplitz matrix built from the Fourier components of the conductivity such that its mn element is given by $\Sigma_{mn} = \sigma_{m-n}$. A rapid comparison between expressions in Eqs. (4)–(6) shows that they have the same structure where the role of η in the former equations is played by $Z_0\Sigma$ in the second set of equations. In the former case, the scattering channels are independent of each other (in the sense that each coefficient b_n depends only on its counterpart of the same order a_n), whereas, in the second case, they are coupled through matrix Σ (i.e., each b_n depends on the set of all a_n coefficients). In the numerical implementation, the series are truncated to a limited number of harmonics usually going from $n = -M$ to $n = M$ such that $N = 2M+1$ coefficients are kept. M is called the truncation order.

B. The FMM with ABCs

In the classical FMM, Laurent's direct rule has been used to Fourier factorize the product $\sigma(\omega,\theta)E_{zi}(R,\theta)$, whereas, it is the inverse rule [11,14] that should be used. Unfortunately, the inverse rule will make use of the reciprocal of the conductivity function, $1/\sigma(\theta)$, whereas, the latter takes infinite values on the part of the circumference without graphene. This clearly forbids the use of such a rule. To circumvent this problem, Khavasi, in the case of planar graphene strip gratings, introduced approximate boundary conditions [10] leading to an effective conductivity whose reciprocal is never infinite, thus, bringing back the possibility to use the inverse rule. Here, we are facing the same situation and, hence, can transpose the work performed in Ref. [10] in cylindrical geometry. To be more specific, let us start from Ampere's law and apply it to the closed rectangular loops (Σ) shown in Fig. 2. Then, for a fixed θ,

$$l\{H_{zi}(R^-,\theta) - H_{zo}(R^+,\theta)\} = \int_{R^-}^{R^+}\int_0^l \{\sigma(\theta)\delta(r-R) - i\omega\varepsilon\}E_\theta(r,\theta)dz\,dr, \tag{7}$$

with $R^\pm = R \pm \Delta/2$, l, and Δ being the width and the height of the contour (Σ). For sufficiently small Δ, $E_\theta(r,\theta)$ can be approximated by $E_{\theta i}(R,\theta)$ [or $E_{\theta o}(R,\theta)$] and taken out of the integral, which leads finally to the ABC,

$$H_{zi}(R^-,\theta) - H_{zo}(R^+,\theta) = \widetilde{\sigma}(\theta)E_{\theta i/o}(R,\theta), \tag{8}$$

where $\widetilde{\sigma}(\theta) = \sigma(\theta) - i\omega\varepsilon_0\Delta(\varepsilon_i+\varepsilon_o)/2$ is the effective surface conductivity (depending on the new parameter Δ) that, now, never goes to zero. It is now possible to use the inverse rule for this ABC which combined with the continuity of the electric field leads to the new expressions of the scattering coefficients that are exactly those of Eq. (5) where the matrices A and B are replaced by

$$A = n_i \widetilde{J}_i J_o' - n_o \widetilde{J}_o J_i' + iZ_0 J_i' \widetilde{\Sigma}^{-1} J_o',$$
$$B = n_o \widetilde{H}^+ J_i' - n_i \widetilde{J}_i H^{+'} - iZ_0 J_i' \widetilde{\Sigma}^{-1} H^{+'}, \tag{9}$$

where $\widetilde{\Sigma}$ is the Toeplitz matrix built from the Fourier components of the reciprocal of the effective conductivity $\widetilde{\sigma}^{-1}(\theta)$. $\widetilde{J}_i = \mathrm{diag}[J_{ni}(k_i R^-)]$, $\widetilde{J}_o = [J_{no}(k_o R^+)]$, and $\widetilde{H}^+ = \mathrm{diag}[H_n^+(k_o R^+)]$.

Although this approach has been shown to be effective (at least, for the far field calculations) for planar diffraction gratings, it appears to experience some problems (as will be shown below) in the case of circular strips especially near sharp resonances that are generally the most interesting spectral zones. The FMM equipped with ABC can ensure convergence, but for that, a suitable choice of Δ is necessary which requires ancillary calculations. In addition, Δ depends on the wavelength. It is for this reason that a new and very efficient method has been proposed in Ref. [12] to model diffraction from planar strips and that we adapt here for cylindrical strips and present in the following section.

C. The FMM with LBFs

We start from the expressions of the fields in the inner and outer media [Eqs. (2)] and add an expression of the electric field valid on the interface $r = R$, given in terms of the LBFs, $g_m(\theta)$ and $s_m(\theta)$, that reproduce its singularities at $\theta = 0$ and $\theta = \theta_g$,

$$E_\theta(\theta) = \begin{cases} \sum_{m=1}^{N_g} p_m g_m(\theta), & 0 \leqslant \theta \leqslant \theta_g, \\ \sum_{m=0}^{N_s-1} q_m s_m(\theta), & \theta_g < \theta < 2\pi, \end{cases} \tag{10}$$

where

$$g_m(\theta) = \sin(m\pi\theta/\theta_g),$$
$$s_m(\theta) = \cos[m\pi(\theta-\theta_g)/\bar{\theta}_g]/\sqrt{(\bar{\theta}_g/2)^2 - (\theta-\theta_c)^2},$$

p_m and q_m are the associated expansion coefficients, $\bar{\theta}_g = 2\pi - \theta_g$ and $\theta_c = (\theta_g + 2\pi)/2$. Parameters N_g and N_s represent the number of basis functions in the graphene strip and slit regions, respectively. Functions $g_m(\theta)$ are a good choice to

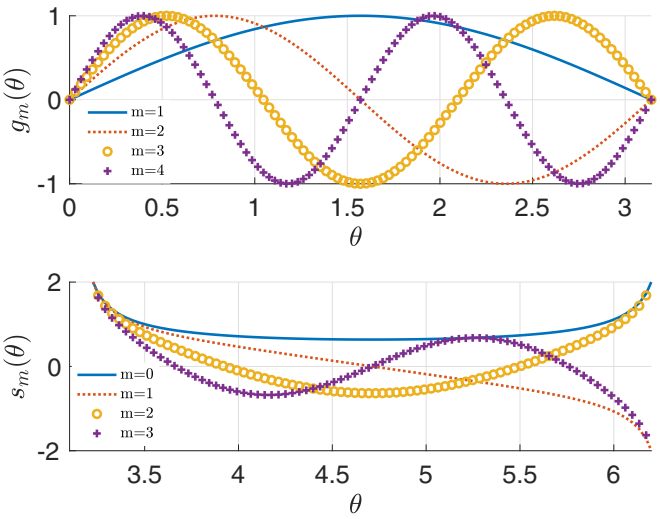

FIG. 3. Shapes of the first four functions (a) $g_m(\theta)$ and (b) $s_m(\theta)$.

represent E_θ over the graphene region ($r = R$ and $0 \leqslant \theta \leqslant \theta_g$) since this component vanishes to zero at the ends of the strip as has been shown in Ref. [10]. In the complementary region ($r = R$ and $\theta_g < \theta < 2\pi$), E_θ presents two singularities at the end points of the interval and are well described through functions $s_m(\theta)$. These functions are shown in Fig. 3.

Now, for the boundary conditions, we must have

$$\begin{aligned} E_{\theta i}(R,\theta) &= E_{\theta o}(R,\theta), \\ H_{zo}(R,\theta) - H_{zi}(R,\theta) &= \sigma(\theta) E_{\theta i}(R,\theta), \\ E_{\theta i}(R,\theta) &= E_\theta(\theta). \end{aligned} \tag{11}$$

The first two equations correspond to the classical boundary conditions used before. As for the third one, it enforces the electric field at $r = R$ to match the one represented by LBFs: $E_\theta(\theta)$. Projecting the first equation on the Fourier basis yields, under matrix form

$$\frac{k_i}{\varepsilon_i} J_i' c = \frac{k_o}{\varepsilon_o}(J_o' a + H^{+'} b). \tag{12}$$

Then, projecting the second and third equations on the same basis gives

$$J_i c - J_o a - H^+ b = \sigma G p, \tag{13}$$

and

$$\frac{-iZ_0}{n_i} J_i' c = Gp + Sq, \tag{14}$$

where p (respectively, q) is the column vector formed by the N_g coefficients p_m (respectively, N_s coefficients q_m). Matrices G and S (with sizes $N \times N_g$ and $N \times N_s$, respectively) are given by $G_{nm} = \langle g_m(\theta), e^{in\theta} \rangle$ and $S_{nm} = \langle s_m(\theta), e^{in\theta} \rangle$, and more specifically,

$$G_{mn} = \frac{-i\theta_g}{4\pi} e^{-i\frac{n\theta_g}{2}} \left[e^{i\frac{m\pi}{2}} \mathrm{sinc}(\alpha_{nm}^-) - e^{-i\frac{m\pi}{2}} \mathrm{sinc}(\alpha_{nm}^+) \right],$$

$$S_{np} = \frac{1}{4} e^{-in\theta_c} \left[e^{i\frac{p\pi}{2}} J_0(\beta_{np}^-) + e^{-i\frac{p\pi}{2}} J_0(\beta_{np}^+) \right].$$

$\alpha_{nm}^\pm = (m\pi \pm n\theta_g)/2$ and $\beta^\pm = (m\pi \pm n\bar{\theta}_g)/2$. Here, we adopt the notation $\mathrm{sinc}(x) = \sin(x)/x$.

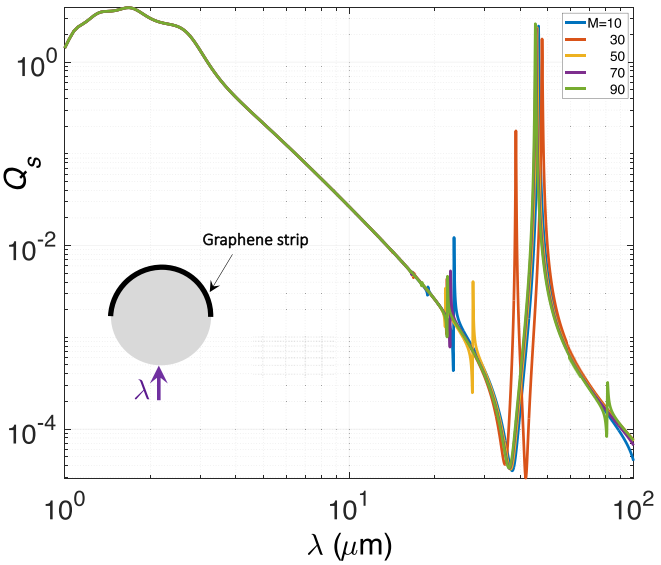

FIG. 4. Scattering efficiency spectrum computed with the classical FMM for different values of the truncation order M.

Solving these algebraic systems leads to expressions of the coefficients b and c that have, once again, the same form as in Eq. (5) where matrices A and B are given by

$$\begin{aligned} A &= n_i J_i J_o' - n_o J_o J_i' + iZ_0 \sigma J_i' W J_o', \\ B &= n_o J_i' H^+ - n_i J_i H^{+'} - iZ_0 \sigma J_i' W H^{+'}. \end{aligned} \tag{15}$$

$W = W_1 W_2^{-1}$, where $W_1 = [G\ \mathbf{0}]$ is the concatenation of matrices G and the matrix $\mathbf{0}$ denoting the zero matrix of size $N \times N_s$ and $W_2 = [G\ S]$ is the concatenation of matrices G and S. Then, coefficients p and q can be obtained simply from Eq. (14).

III. RESULTS

A. Convergence and stability

Let us now compare the performances of the three approaches in terms of convergence and stability when the total number of Fourier harmonics retained in the numerical computations is increased. Such a number will be denoted by $N = 2M + 1$ where M is, usually, called the truncation order. We consider a cylinder with radius $R = 0.5$ μm, lying in vacuum and filled with a dielectric of relative permittivity $\varepsilon_i = 3.9$, it is covered with a sheet of graphene whose parameters are $\theta_g = \pi$, $\mu = 0.5$, $\hbar\Gamma = 0.1$ eV taken at $T = 300$ K. The angle of incidence is first fixed at $\varphi = \pi/2$. Figure 4 shows the spectrum of the scattering efficiency computed with the classical FMM approach for different truncation orders. We can clearly distinguish two subdomains in this spectrum: a low wavelength subdomain where the method seems to behave properly and a high wavelength subdomain where there are some resonances (due to surface plasmons polaritons on graphene [15]) and where the method fails to converge. This manifests as many spurious and unstable peaks and dips appearing in this region of the spectrum. It is of fundamental importance to emphasize that increasing further the truncation order does not lead to any stabilization of these resonances. As

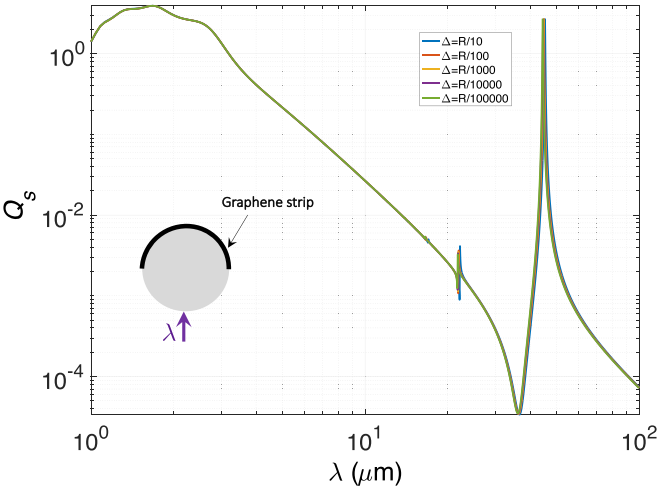

FIG. 5. Scattering efficiency spectrum computed with the FMM-ABC for different values of Δ and for a truncation order: $M = 90$.

stated in the theoretical section, this lack of convergence was expected for the classical FMM (it is due to the improper use of the correct Fourier factorization rules, cf. Refs. [10,11]) and is clearly demonstrated in these calculations.

Now, let us examine the behavior of the FMM with ABCs and explore the influence of the free parameter Δ. Figure 5 shows the scattering efficiency spectrum computed for different values of Δ and for $M = 90$, which is a rather high truncation order. First, we observe far better convergence and stability behaviours as compared to the classical FMM. Second, we clearly see the predominance of two main peaks keeping almost the same spectral positions, in contrast with the former results. A closer look at these peaks, reported in Fig. 6, reveals that they shift towards low wavelengths as the parameter Δ is decreased, and seem to converge to specific positions.

To clarify this last point, we focus on the rightmost peak and follow the evolution of its wavelength λ_p as the parameters M and Δ are varied. The results are shown in Fig. 7 where we plot λ_p versus M for three different values of Δ. For each value of Δ, we observe a convergence process leading to different values of λ_p. For comparison we added, in Fig. 7, the results obtained by use of the FFM-LBF (magenta solid line with squares) which show a clear and fast convergence to $\lambda_p \simeq 44.86$ μm which we will consider as the reference value [12].

Thus, we see that the FMM-ABC can predict quite correctly the shape and the number of resonances but presets stability problems regarding the peaks associated with resonant phenomena in the structure. This is linked to the difficulty of choosing the right Δ, all the more so that this latter may vary with the wavelength. For the FMM-LBF, on the contrary, there is no supplementary parameters involved, and the method proves to be stable against the positions of sharp resonances. It is worth emphasizing that, from our numerical experiments, the same conclusion holds for the lower wavelength peak ($\lambda_p \simeq 21.93$ μm). From the standpoint of convergence, the superiority of the FMM-LBF is evident as can be seen from Fig. 8 where we plot the scattering effi-

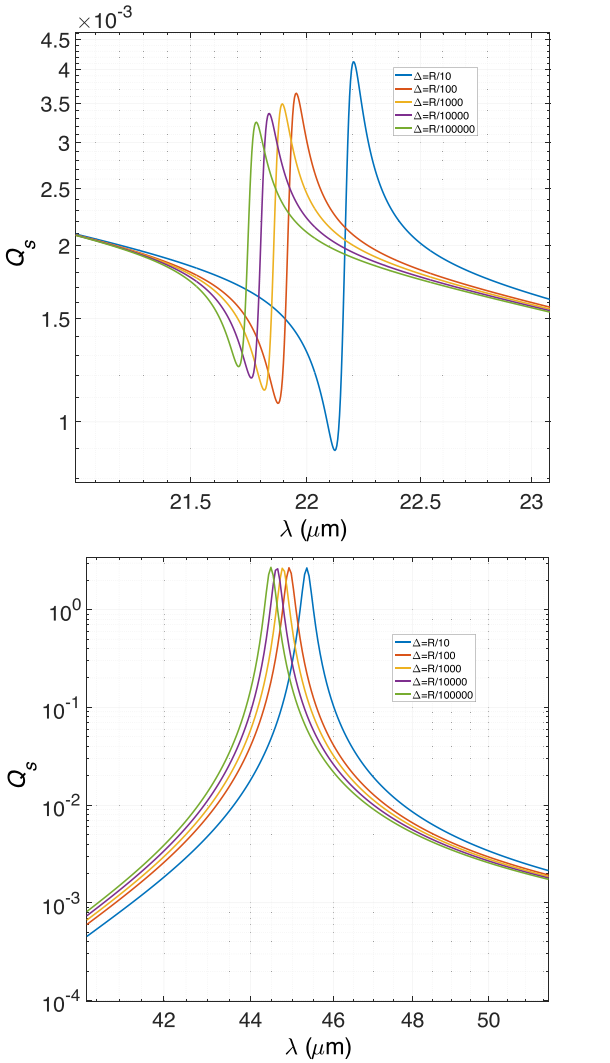

FIG. 6. Zooms over the two main resonances observed in Fig. 5. Left around 22 μm and right around 45 μm.

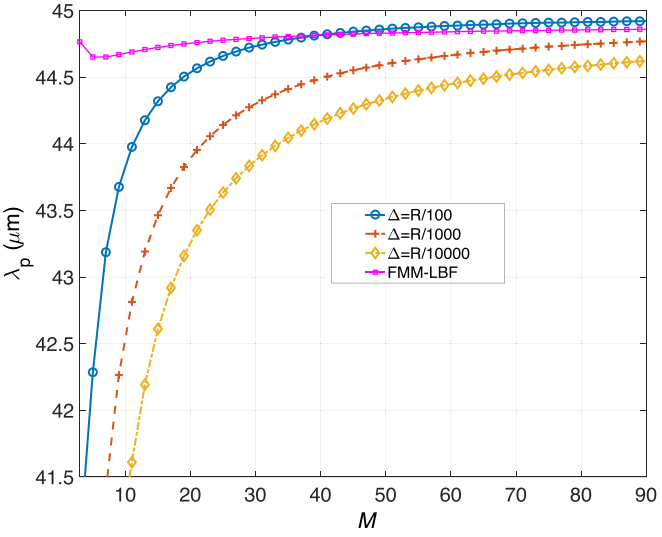

FIG. 7. Evolution of the rightmost peak wavelength λ_p versus M for different values of Δ.

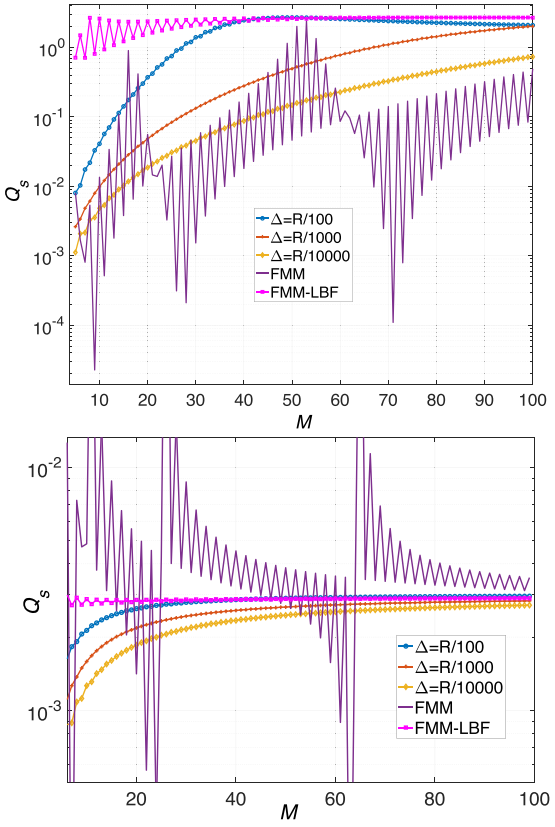

FIG. 8. Q_s versus M at resonance for $\lambda = 44.86$ μm (upper panel) and out of resonance for $\lambda = 50$ μm (lower panel).

ciency versus the truncation order M for two wavelengths (at resonance and out of resonance) computed with the classical FMM, the FMM-ABC, and the FMM-LBF. The FMM (solid purple line) is completely out of convergence for both cases whereas the FMM-ABC behaves slightly better but still presents the Δ choice problem. The FMM-LBF shows clear convergence for both wavelengths and is even faster for the out of resonance case. Therefore, and because of its outstanding performances, the FMM-LBF will be our tool for investigating the physics behind the observed resonances in the considered structure.

B. Plasmonic modes over the graphene strip

We would like, now, to examine the physical origin of the resonances observed in the scattering efficiency spectrum. For that, we first compute (using the FMM-LBF) and report in Fig. 9, the scattering efficiency spectrum together with the modulus of the smallest eigenvalue of matrix B of Eq. (15) (rescaled for more clarity). The magnitude of this latter presents dips almost wherever the structure has a mode. We observe that there are more modes than what can be observed in the scattering efficiency spectrum. This is due to the lack of compatibility between the absent modes and the symmetry of the physical configuration. To gain more insight, we plot the map of the modulus of the electric component $E_\theta(x, y)$ around the coated cylinder for the four first resonant peaks observed in the spectrum: $\lambda_1 = 44.86$, $\lambda_3 = 21.93$, $\lambda_5 = 16.66$, and $\lambda_7 = 13.98$ μm (note that the last two peaks are tiny

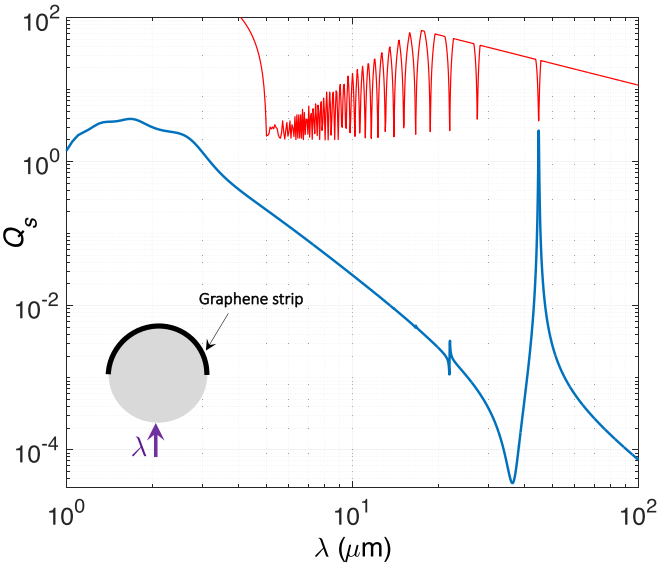

FIG. 9. Scattering efficiency computed with the FMM-LBF (blue) for $M = 90$. The red curve represents the modulus of the smallest eigenvalue of matrix B of Eq. (15) (rescaled for the clarity of the figure).

and hardly observable in Fig. 9). The results are depicted in Fig. 10 where we first note the expected singular behavior at the ends of the graphene sheet (namely, at $\theta = 0$ and $\theta = \pi$). The different peaks represent the plasmonic resonances [15] supported by the graphene sheet at these wavelengths, and it is of fundamental importance to remark that they all have an odd number of antinodes (1, 3, 5, and 7, hence, their numbering) because of the symmetry of the physical configuration. The other plasmonic resonances (with an even number of antinodes) can be excited if we change the angle of incidence to be compatible with these modes. An example of such a situation is given in Fig. 11 where we took an angle of incidence

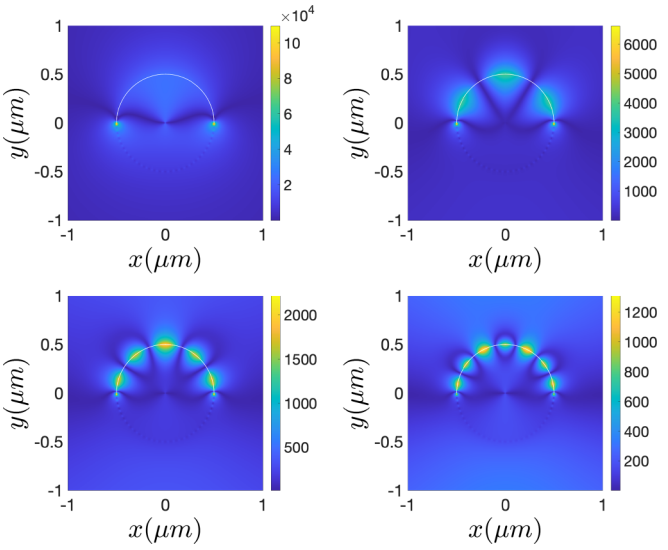

FIG. 10. Map of the modulus of the electric component $E_\theta(x, y)$ computed for the four first resonant peaks observed in the spectrum of Fig. 9: $\lambda_1 = 44.86$, $\lambda_3 = 21.93$, $\lambda_5 = 16.66$, and $\lambda_7 = 13.98$ μm.

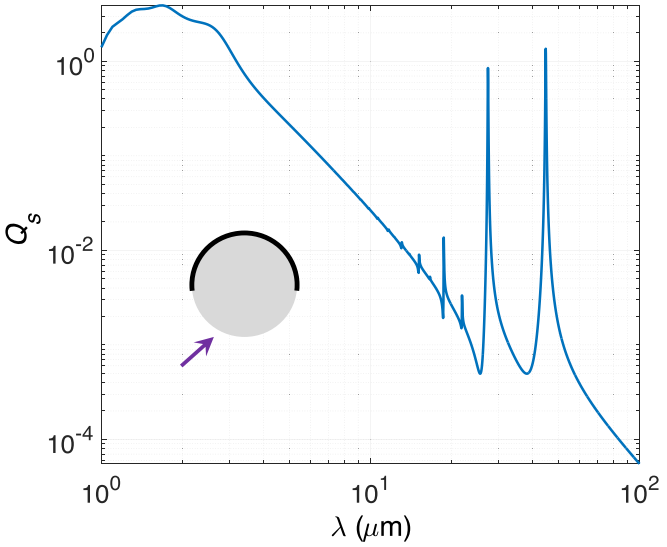

FIG. 11. Scattering efficiency spectrum computed with the FMM-LBF at an incidence $\varphi = \pi/4$ with $M = 90$, and the other parameters are unchanged.

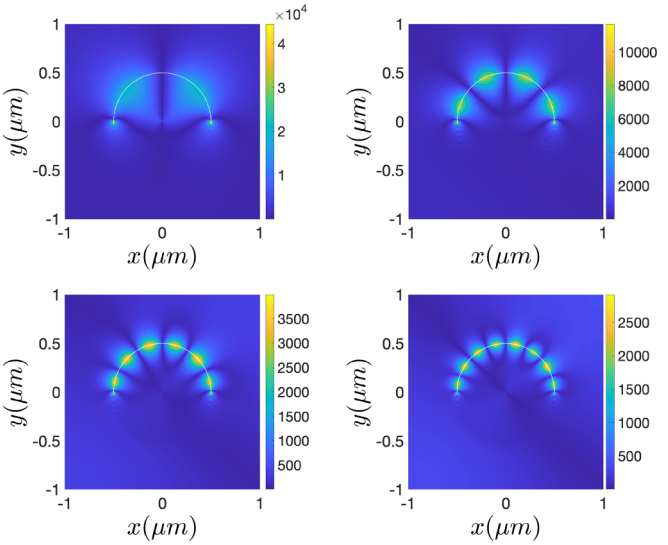

FIG. 12. Map of the modulus of the electric component $E_\theta(x, y)$ computed for the new resonant peaks appearing in the spectrum of Fig. 11: $\lambda_2 = 27.34$, $\lambda_4 = 18.72$, $\lambda_6 = 15.16$, and $\lambda_8 = 13.07$ μm.

$\varphi = \pi/4$ and computed a new spectrum clearly revealing the missing plasmonic peaks. To complete the picture, we report in Fig. 12 the map of the modulus of the electric component $E_\theta(x, y)$ for the peaks $\lambda_2 = 27.34$, $\lambda_4 = 18.72$, $\lambda_6 = 15.16$, and $\lambda_8 = 13.07$ μm.

IV. CONCLUSION

We presented an efficient and numerically very robust approach for the modeling of EM scattering from a cylinder partially covered with graphene. It is based on the classical Fourier-Bessel decomposition and classical boundary conditions to which we adjoint an *ad hoc* expansion of the tangential electric field valid over the circumference. This latter is introduced to better take into account the singular nature of this field at the ends of the graphene sheet. Using this method, we explored the scattering efficiency spectra of such structures and and showed that they present several peaks that we related to the existence of surface plasmon polariton modes over graphene. The nature of each mode has been examined through the computation of the near field map of the electric field that revealed their standing wave nature. This method can be, safely, used in the study of the properties of this kind of setups exhibiting superscattering or invisibility, for example. Finally, it of interest to stress that it can be easily extended to multilayered cylinders with many strips at each interface which will allow a much more richer behavior.

[1] J. A. Kong, *Electromagnetic Wave Theory* (Wiley, New York, 1986).

[2] Z. Ruan and S. Fan, Superscattering of Light from Subwavelength Nanostructures, Phys. Rev. Lett. **105**, 013901 2010.

[3] R. Li, B. Zheng, X. Lin, R. Hao, S. Lin, W. Yin, E. Li, and H. Chen, Design of ultracompact graphene-based superscatterers, IEEE J. Select. Topics Quantum Electron. **23**, 4600208 (2017).

[4] B. Guizal and D. Felbacq, Numerical computation of the scattering matrix of an electromagnetic resonator, Phys. Rev. E **66**, 026602 (2002).

[5] S. V. Dukhopelnykov, R. Sauleau, M. Garcia-Vigueras, and A. I. Nosich, Combined plasmon-resonance and photonic-jet effect in the THz wave scattering by dielectric rod decorated with graphene strip, J. Appl. Phys. **126**, 023104 (2019).

[6] S. V. Dukhopelnykov, R. Sauleau, and A. I. Nosich, Integral equation analysis of terahertz backscattering from circular dielectric rod with partial graphene cover, IEEE J. Quantum Electron. **56**, 8500208 (2020).

[7] A. Taflove, *Computational Electrodynamics: The Finite-Dfference Time-Dmain Method* (Artech House, New York, 1995).

[8] F. Bengzon and M. G. Larson, *The Finite Element Method: Theory, Implementation, and Applications* (Springer, Berlin/Heidelberg, 2015).

[9] B. Guizal and D. Felbacq, Electromagnetic beam diffraction by a finite strip grating Opt. Commun. **165**, 1 (1999).

[10] A. Khavasi, Fast convergent Fourier modal method for the analysis of periodic arrays of graphene ribbons, Opt. Lett. **38**, 3009 (2013).

[11] L. Li, Use of Fourier series in the analysis of discontinuous periodic structures, J. Opt. Soc. Am. A **13**, 1870 (1996).

[12] R.-B. Hwang, Highly improved convergence approach incorporating edge conditions for scattering analysis of graphene gratings, Sci. Rep. **10**, 12855 (2020).

[13] L. A. Falkovsky, Optical properties of graphene, J. Phys.: Conf. Ser. **129**, 012004 (2008).

[14] G. Granet and B. Guizal, Efficient implementation of the coupled-wave method for metallic lamellar gratings in tm polarization J. Opt. Soc. Am. A **13**, 1019 (1996).

[15] M. Naserpour, C. J. Zapata-Rodríguez, S. M. Vuković, H. Pashaeiadl, and M. R. Belić, Tunable invisibility cloaking by using isolated graphene-coated nanowires and dimers, Sci. Rep. **7**, 12186 (2017).